Microstructural analysis and mechanical properties of concrete reinforced with polymer short fibers.

Anton Trofimov[1], Tatiana Mishurova[2], Luca Lanzoni[3], Enrico Radi[3], Giovanni Bruno[2], Igor Sevostianov[4*]

[1] Center for Design, Manufacturing, and Materials, Skolkovo Institute of Science and Technology, Skolkovo, Russia
[2]BAM, Bundesanstalt für Materialforschung und –Prüfung, Unter den Eichen 87, Berlin 12205, Germany
[3]Dipartimento di Scienze e Metodi dell'Ingegneria, Università di Modena e Reggio Emilia, Via Amendola, 2 Reggio Emilia 42122, Italy
[4] Department of Mechanical and Aerospace Engineering, New Mexico State University, Las Cruces, NM (USA)

***Corresponding author**

ABSTRACT

The paper focuses on the quantitative characterization of a concrete containing polymer fibers and pores. Computed tomography (CT) characterization technique is used to provide input data for Finite Element Method (FEM) simulations and analytical modeling based on micromechanical homogenization via the compliance contribution tensor formalism. Effective elastic properties of reinforced concrete are obtained experimentally using compression testing, analytically in the framework of Non-Interaction approximation and numerically performing direct FEM simulations on specimen with reconstructed microstructure. It is shown that CT produces results suitable for implementation in numerical and analytical models. The results of analytical and numerical modeling are in a good agreement with experimental measurements providing maximum discrepancy of ~ 2.5%.

Keywords: reinforced concrete; computer tomography, Finite Element Method, micromechanics, homogenization

1. Introduction.

In countries such as Italy, Greece, and Turkey, earthquakes may create large and diffuse damage to existing buildings, depending on the amplitude and frequency content of the earthquake. An innovative technology for vibration control and risk mitigation of reinforced concrete (RC) structures in this area consists in the use of fibre reinforced concrete (FRC) instead of plain concrete. Mechanical performances of FRC are largely improved with special references to dissipative properties under seismic loads [1,2]. In particular, synthetic fibres are expected to enhance the dynamic properties of concrete by improving the strength, ductility, and toughness of plain concrete, as well as its damping ratio (e.g. [3,4]). Since the concrete matrix is generally stiffer than the reinforcing synthetic fibers, their addition to the concrete mix may also reduce the elastic stiffness of FRC structures, thus lowering their fundamental natural frequencies.

The overall properties of FRC strongly depend on the volume fraction of fibres added to the matrix, as well as on their distribution and orientation. To achieve the best FRC performance, the synthetic fibres should also display good chemical compatibility with cement matrix, thus possessing proper bond characteristics. However, due to their chemical inertia, polymeric materials usually display poor adhesion to the cement matrix [5]. In order to enhance the adhesion of synthetic fibres to the cement matrix, several approaches have been proposed such as giving a suitable shape to fibres that may increase the grip [4,6,7]. Recently, an innovative method of chemical nature (based on a nano-Silica surface treatment) has been proposed for improving the bonding of polypropylene (PP) fibres with the hydration products of the cement matrix [8,9]. The proposed treatment has generally a positive effect on the bending strength and other mechanical properties of FRC [10]. In particular, the relatively high tensile strength of synthetic fibres contributes to withstanding the crack initiation stress and resisting pull out force. This is due to the strong bond between the fibre and the cementitious matrix [9,11]. Moreover, due to the reduced elastic modulus, synthetic fibres may elongate under loading and transfer the load to different parts of the matrix. As a result, the load applied is distributed more evenly along the interface between fiber and matrix [12].

The main objective of the current study is to investigate the influence of discrete PP fibre addition on the mechanical properties of FRC by using the combined techniques of computed tomography (CT), FEM analysis, and micromechanical modelling, focusing on its effective elastic properties. PP draw-wired fibres of geometric length of 18 mm with diameter of 0.28 mm at a typical weight dosage of 0.25% were utilised. Static mechanical properties of FRC (*i.e.* stress *vs* strain curves, ultimate compressive strength, indirect tensile strength, modulus of rupture and modulus of elasticity) at the age of 28 days were also measured and results compared with that of reference concrete.

Laboratory X-ray Computed Tomography (CT) is an increasingly widely used non-destructive testing technique in concrete research. It allows locating and even quantifying internal structures and defects in concrete (*e.g.*, aggregates, pores, reinforcement) in 3D. Especially, in the case of complex structures like FRC, CT is a useful tool for the evaluation of spatial and orientation distribution of fibres [13–15]. Also the damage in concrete after and during (*i.e.*, *in-situ*)

mechanical tests can be estimated [16,17]. Additionally, 3D image date from tomography could be used as input for analytical [18] and numerical models [19], improving the prediction of mechanical behaviour of the concrete.

The paper is organized as follows. Samples preparation is described in Section 2, mechanical testing results are summarized in Section 3. CT measurements are reported in Section 4, analytical and numerical modelling procedures are discussed in in Section 5. Finally, the main results obtained by the analyses are reported and discussed in Section 7.

2. Specimens preparation and mechanical testing

Fiber reinforced concrete (FRC) beam-like specimens 150 mm deep, 150 mm wide and 600 mm long were cast and cured according to UNI 12390-1:2002 and UNI EN 12390-2:2002. The mix design adopted for the concrete mixture is given in Table 1. Cement and aggregates used for realizing samples accomplish regulations UNI EN 197-1:2011 and UNI EN 12620:2008, respectively. Note that only fine aggregates with size in the range 0÷4 mm have been used in the FRC samples. This avoids significant scale effects on small samples when subjected to mechanical tests (see Section 3).

Polypropylene discrete draw-wired fibers were incorporated in the mixture at the mixing stage at a dosage of 2.5 kg/m^3, that corresponds to a volume fraction of about 0.25%. The aspect ratio of fibers (i.e. the ratio of the length to equivalent diameter ratio) is 65. The main physical and mechanical properties of fibers are reported in Table 2.

Table 1 Plain concrete composition used to realize the samples

Cement		Aggregates, kg/m^3		Water	Ratio w/c
type	kg/m^3	0-2,mm	2-4,mm	kg/m^3	0.56
CEM II 42.5 R	315	1080	800	175	

Table 2. Properties of polypropylene fibers

L, mm	Diameter, mm	ρ , kg/m^3	σ_{TS} , MPa	E ,GPa
18	0.28	1000	300	2.2

After a curing period of 28 days, beam-like 150 mm x 150 mm x 600 mm specimens have been sawed to small ones - 18 x 18 x 60 mm^3 and 18 x 18 x 25 mm^3 suitable for CT using electromechanical blade (see Figure 1). Specimens were sawed longitudinally, *i.e.*, along the main direction of the beam highlighted in red in Figure 1.

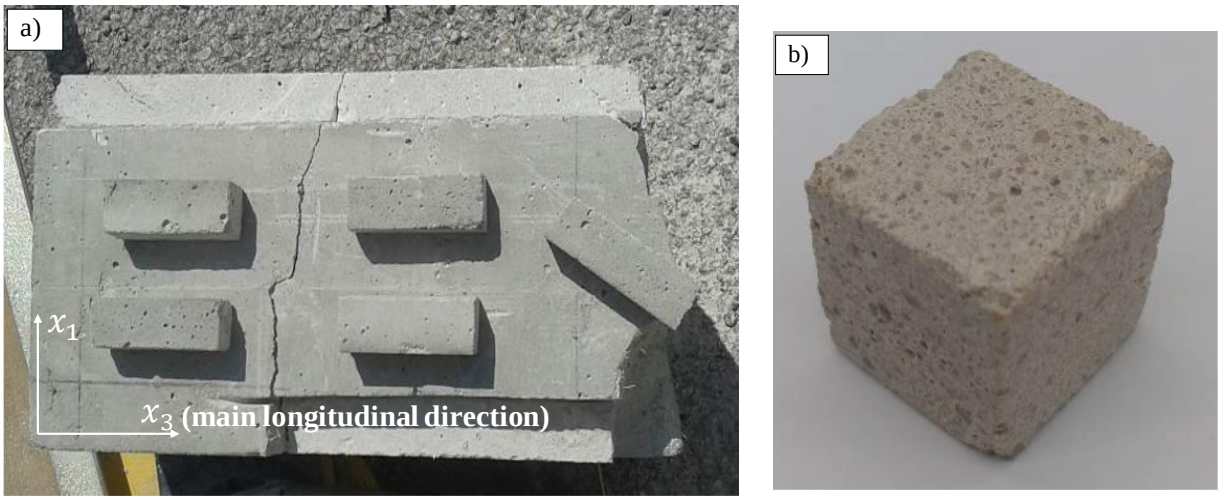

Figure 1. a) Prismatic 18 x 18 x 60 mm^3 and b) 18 x 18 x 25 mm^3 specimens obtained by cutting 150 x 150 x 600 mm^3 concrete specimens.

In order to characterize the mechanical properties of FRC, another group of specimens has been prepared for compressive tests. The mechanical tests were performed according to the standard UNI EN 1015-11:2001 for cementitious mortars. Accordingly, the compression load was applied through a load cell at a load rate of 50 N/s. Four 18 x 18 x 25 mm^3 specimens were subjected to compression until complete failure (Figure 2). In order to investigate the effect of fibers orientation, two specimens were tested by applying the load parallel (P1, P2) to the main axis of the beam-like specimen, whereas other two samples were subjected to a compressive load acting transversally (T1, T2) to it.

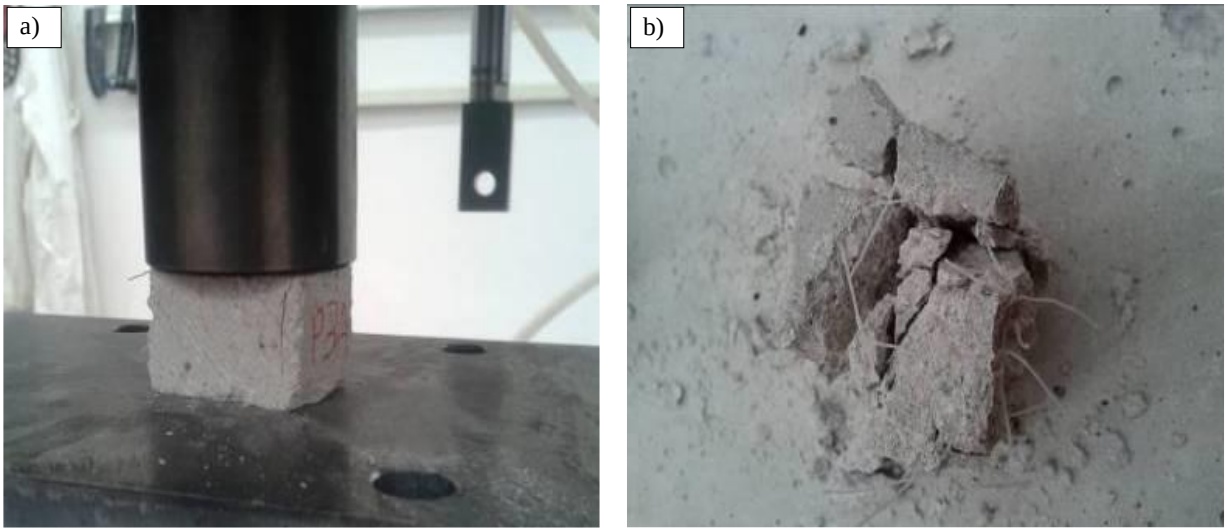

Figure 2. Prismatic 18 x 18 x 25 mm samples a) before and b) after the compression test.

The stress-strain curves obtained in the compression test are shown in Figure 3. Note that in Fig.3 the starting/reference point for displacement was shifted to account for the machine compliance. As expected, the ultimate strength along the direction parallel to the beam-like specimen (P), that equals 42 MPa, is greater than the strength in the transverse direction (T), which is of the order of 35 MPa. Interestingly, the displacement at rupture (the so-called strain tolerance) is the same in all the cases. The slope of the σ/ε curves is almost the same for all the specimens in the range of the axial relative displacement up to 0.01. Making reference to such a range, the corresponding Young modulus turns out to be 1.7 MPa.

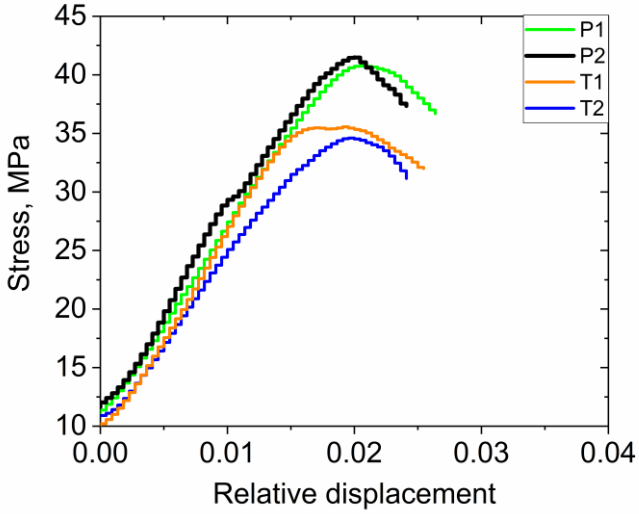

Figure 3. Stress *vs* strain curves obtained by compression tests of 18 x 18 x 25 mm^3 samples.

3. Computed tomography.

The CT measurements were carried out by using a v|tome|x L 300 CT scanner from General Electric. During each scan, 3150 projections were acquired with the acquisition time of 2 sec for each projection. An acceleration voltage of 120 keV and a tube current of 115 µA were used throughout the experiments. A voxel size of around 17 µm was used. The typical resolution of laboratory CT very well suites investigations of the microstructure of inhomogeneous materials such as concrete or asphalt, which possess inhomogeneities of the order of 100 µm (or larger).

Image analysis of the reconstructed volumes was performed using Amira ZIB Edition from the Konrad-Zuse-Zentrum Berlin [13]. Pores were segmented by global threshold. Due to low contrast between polymer fibers, matrix, and pores, identification of fibers was performed by tracing fibers by means of a template matching algorithm. This algorithm generates correlation and orientation fields by matching the reconstructed volume with a cylindrical template, which is defined by user. Additionally, the position of every point of a fiber, as well the fiber spatial and angular orientation, was extracted and used as input for numerical simulation.

An example of a slice of the reconstructed volume data obtained by CT for prismatic sample in transversal direction is presented in Figure 4. Fibers could be distinguished from pores by means

of their ellipsoidal cross section and higher gray value (Fig.4a). 3D rendering and equivalent diameter distribution histogram of pores are presented in Fig 4b and c, respectively. The volume fraction of pores was around 3.8%. The maximum pore diameter reached around 3 mm, however only a few pores with diameter more than 2 mm were found. The pore diameter distribution was used as input in FEM simulation.

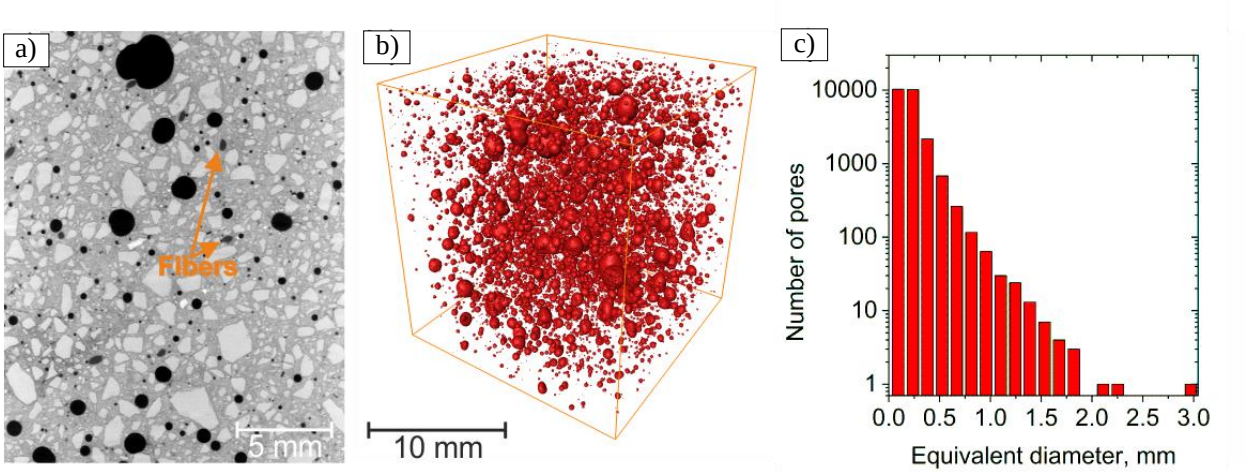

Figure 4: a) 2D reconstructed slices from CT measurements b) 3D rendering of pores c) equivalent diameter pore distribution histogram.

Traced fibers, obtained by the template matching algorithm and colored according to their angular orientation, are presented in Fig. 5a,b. The orientation of fibers was determined in spherical coordinates by angles θ and φ (see Fig. 5e).

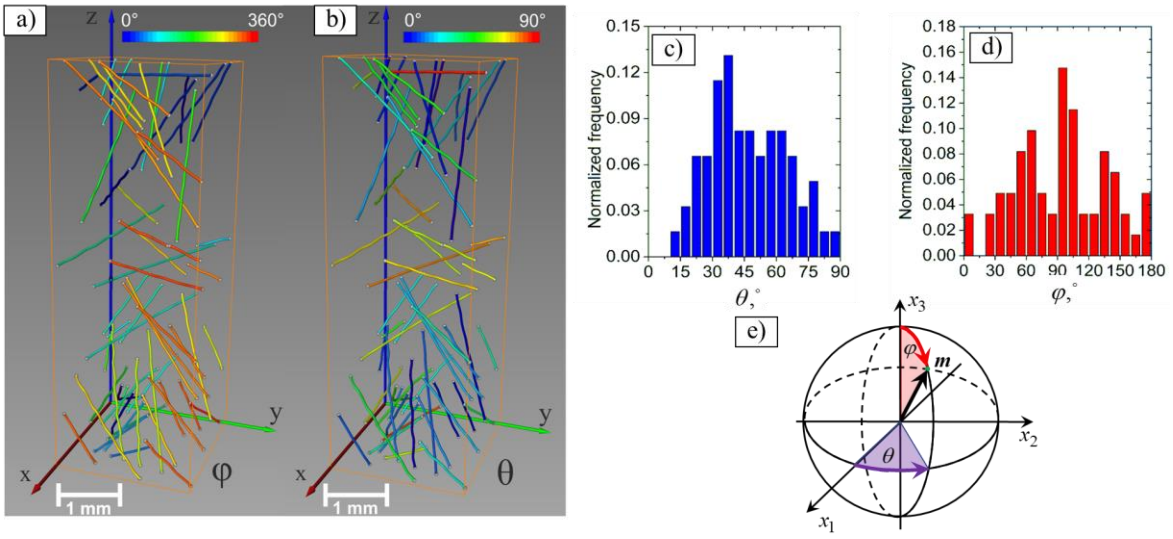

Figure 5. 3D visualization of fiber orientation distribution obtained by CT measurements for angle a) φ and b) θ; orientation distribution histograms for c) θ and d) φ; e) coordinate system

5. Modeling.

The spatial and angular distributions of fibers has been introduced into the FEM simulation and micromechanical modeling. It could seem that orientation distribution histograms (Fig. 5c, d)

show preferential orientation of fibers around 90° for φ angle (angle around the main longitudinal axis) and 40° for θ (tilt from the longitudinal axis). These histograms, however, show the product of appearance frequency with sin φ (see [14]). Taking into account the previous statement and in view of the limited statistics we can ,actually, assume an isotropic distribution of fibers with a good accuracy.

5.1. FEM

Numerical modeling of three-dimensional specimens presents significant challenges related to the conversion of the experimental data into a robust FE mesh, preserving accurate and realistic microstructure representation. In this paper, we consider a polypropylene fiber reinforced concrete block (with pores), which is 46.5 mm thick and has in-plane dimensions of 18x18mm. As an input to our procedure we have specimen dimensions, volume fraction of pores and their size distribution (Fig. 4c), microtomography data including number of fibers, location of control points associated with specific fibers (Fig. 5), and mechanical properties of the constituents. To prepare the necessary 3D mesh for the analysis, we begin by generating the surface mesh of the specimen in a custom MATLAB script as follows. First, we generate a fiber surface mesh using experimentally obtained radius, length, and fiber points. This is done by creating the profiles (circles) of the fiber cross section. Note that points are distributed non-uniformly, therefore, we generate an additional set of points, using interpolation, to have the desired mesh size and quality (Fig 6a). Since profiles are stored as ordered lists of point coordinates, they can be easily connected into triangular elements to produce a continuous FEA surface mesh of the fiber [20,21] (Fig 6a).

Second, we generate pores with given size distribution and volume fraction inside the reference volume, where fibers are already present. To generate a microstructure containing multiple inhomogeneities of desired shapes and sizes for FEM, these inhomogeneities should be packed in a constrained volume without interpenetrations. This numerical task is non-trivial and requires a robust solution algorithm to detect and prevent penetration between inhomogeneities. In our paper, we use an algorithm based on the modified collective rearrangement method developed in [22,23], further modified for spherical pores of a distinct size [24]. As an input to the procedure, we specify the number of phases, shapes, and volume fraction inhomogeneities corresponding to each phase, type of distribution, and orientation. In our case, we have spherical pores and fibers that are of the non-ellipsoidal shape and, thus, we substitute them with circumscribing ellipsoid. Note, that in the algorithm fibers remain fixed and only spheres are subjected to the rearrangement. At the next stage, we generate spherical pores according to the input, and remove undesired collisions by finding each pair of potentially overlapping shapes using k-means tree algorithm [25] and calculating the shortest displacement vector to separate them [26]. Once we obtain all displacement vectors, we apply them at once, and repeat this iterative procedure until an interpenetration-free arrangement is obtained. We then replace ellipsoids with their original shape if it is necessary (Figure 6b). The prepared surface mesh is then placed inside the reference volume and this setup is auto meshed with tetrahedral 3D elements, using commercial software Marc/Mentat (Figure 7).

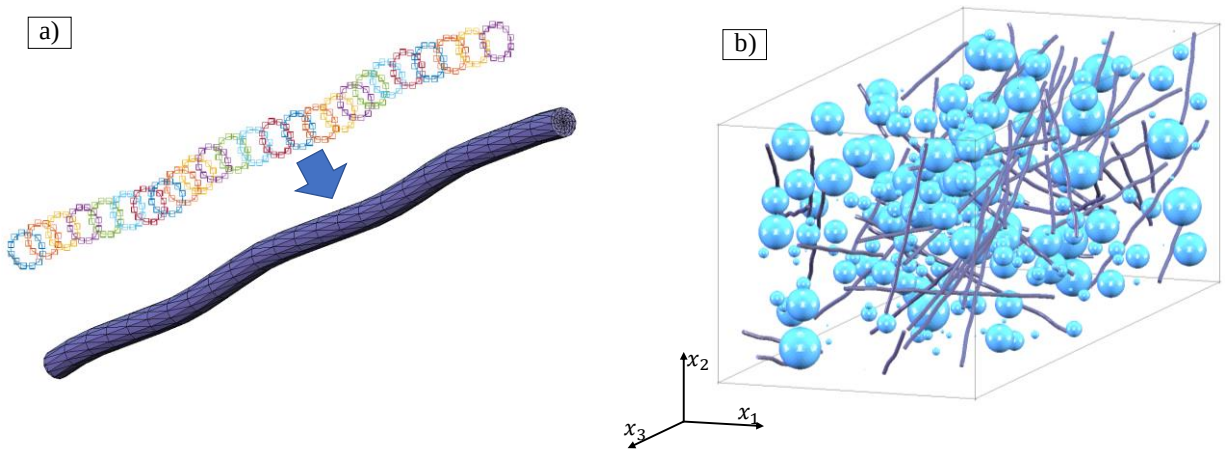

Figure 6. (a) Surface mesh generation procedure for an individual fiber; (b) final structure containing fibers and spherical pores

To determine the effective properties of the specimen we apply a set of six load cases: three uniaxial tension and three shear cases. The boundary conditions for each load case are applied in terms of displacements that correspond to the prescribed values of macroscopic strains $\boldsymbol{\varepsilon}^0$. Once the boundary conditions are prescribed, the FEA simulations are performed, and the resultant files are processed using a custom Python script to determine the overall compliance tensor. The script starts with calculating the average stress components within the volume for each load case:

$$\left\langle \sigma_{ij} \right\rangle_m = \frac{1}{V} \sum_{l=1}^{N} \left(\sigma_{ij}^{(l)} \right)_m \cdot V^{(l)}, (i, j = 1,2,3; k = 1,2,...,6), \tag{5.1}$$

where $\left\langle \sigma_{ij} \right\rangle_m$ is the volume average of the stress component ij calculated from the results of the m-th load case, V is the volume, $\left(\sigma_{ij}^{(l)} \right)_m$ is the stress component ij at the centroid of the finite element l calculated from the m^{th} load case correspondingly, $V^{(l)}$ is the volume of the element l, and N is the total number of elements in the model.

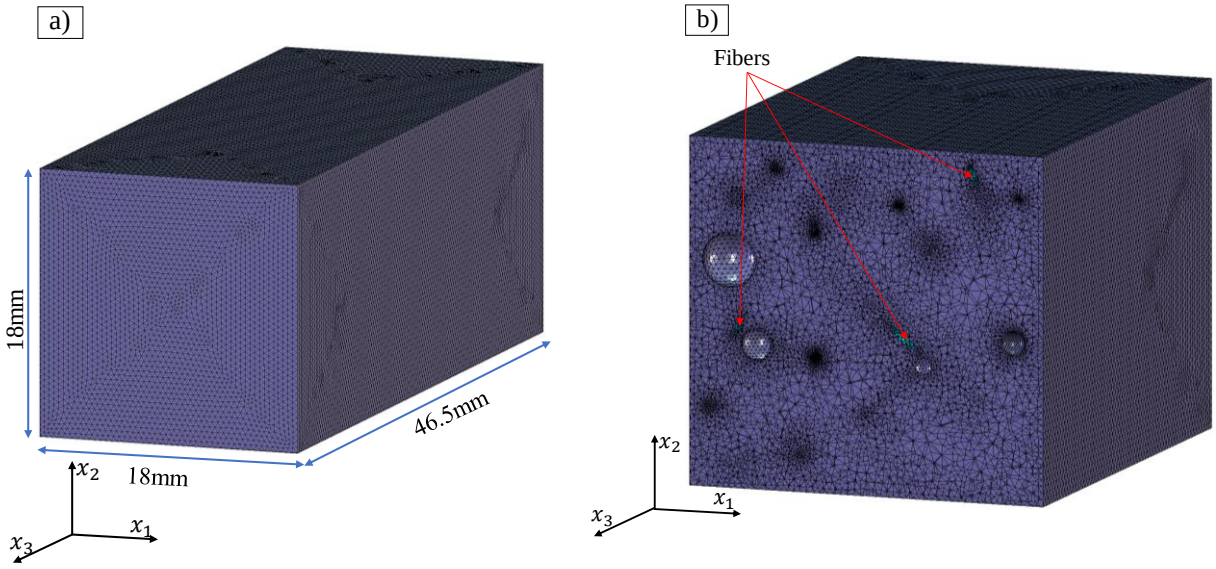

Figure 7. FEM representation of (a) considered specimen; (b) internal mesh structure

Given the average stress we then calculate the components of compliance tensors as follows:

$$S_{ijkl}^{eff} \left\langle \sigma_{ij} \right\rangle_m = (\varepsilon_{kl}^0)_m , \tag{5.2}$$

where ε_{kl}^0 are prescribed components of strain. From the effective compliance, one can obtain engineering constants using Hooke's law. In our simulations, fibers and concrete are assumed and have Young's moduli of 2.2 GPa and 2 GPa, Poisson's ratios of 0.2 and 0.1, correspondingly. The total number of randomly oriented spherical pores with given size distribution to cover the experimentally detected volume fraction of 3.8% is ~300, the number of fibers in composite is 61, the system contains approximately 6.2 million of elements. For the numerical analysis, we developed a robust algorithm for transferring experimental data to the accurate FEM models capturing the main features of the real structure. Table 3 presents the effective elastic constant obtained numerically (see below).

5.2. Micromechanical modeling.

In this section, we use the concept of compliance contribution **H**-tensors of individual shapes to estimate the effective elastic properties of a material containing randomly oriented spherical pores, as well as fibers located and oriented according to the CT data. Compliance contribution tensors have been first introduced in the context of pores and cracks by [27]. For the general case of ellipsoidal elastic inhomogeneities, these tensors were formally defined and calculated by [28,29]. Following these works, we consider a homogeneous elastic material (matrix), with compliance tensor $\mathbf{S}^0$, containing an inhomogeneity, of volume V_1, of a different material with compliance tensor $\mathbf{S}^1$. The compliance contribution tensor of the inhomogeneity is a fourth-rank tensor $\mathbf{H}$ that gives the extra strain (per reference volume V) due to its presence:

$$\Delta\varepsilon_{ij} = \frac{V_1}{V} H_{ijkl}\sigma^0_{kl}, \tag{5.3}$$

where σ^0_{kl} are remotely applied stresses that are assumed to be uniform within V in the absence of the inhomogeneity. For a prolate spheroid (fiber) tensor $\boldsymbol{H}$ has the following form (see book of [30] for details)

$$H^f_{1111} = \frac{1}{2\Delta}\left(K_* + \frac{4}{3}G_* + 4G_0\kappa\right) + \frac{1}{2\left(2G_* + G_0\kappa\right)};\ H^f_{3333} = \frac{2}{\Delta}\left(K_* + \frac{1}{3}G_* + G_0\kappa\right)$$

$$H^f_{1122} = \frac{1}{2\Delta}\left(K_* + \frac{4}{3}G_* + 4G_0\kappa\right) - \frac{1}{2\left(2G_* + G_0\kappa\right)};\ H^f_{1313} = \frac{1}{2\left(2G_* + G_0\right)}$$

$$H^f_{1133} = -\frac{1}{\Delta}\left(K_* - \frac{2}{3}G_* + G_0\left(2\kappa - 1\right)\right)$$

where $\Delta = 2\left[3G_*K_* + G_0\left(2+\kappa\right)K_* + G_0\left(4\kappa - 1\right)\left(G_0 + \left(4/3\right)G_*\right)\right]$ and G_*, K_* are given by

$$K_* = K_1K_0/\left(K_0 - K_1\right), \quad G_* = G_1G_0/\left(G_0 - G_1\right) \tag{5.4}$$

K_0 and K_1 and G_0 and G_1 are bulk and shear moduli of matrix and inhomogeneities, respectively and $\kappa = 1/\left[2(1-\nu_0)\right]$.

For a spherical pore

$$H^p_{ijkl} = \frac{15\left(1-\nu_0\right)}{2G_0}\left[\frac{1}{7-5\nu_0}\left(\frac{1}{2}\delta_{ik}\delta_{jl} + \frac{1}{2}\delta_{il}\delta_{jk} - \frac{1}{3}\delta_{ij}\delta_{kl}\right) + \frac{1}{10\left(1+\nu_0\right)}\ \frac{1}{3}\delta_{ij}\delta_{kl}\right] \tag{5.5}$$

To calculate the overall elastic compliances, we neglect the interaction between the inhomogeneities (that gives reasonably accurate results for volume fraction up to 15-20%, [31]) and characterize the contribution of multiple fibers and pores to the effective elastic properties of the FRC, we sum up contribution from the pores with contribution from the fibers averaged over all possible orientations $\tilde{H}^f_{ijkl}$ which is characterized by two components, for example

$$\tilde{H}^f_{1122} = \frac{1}{30}\left(2H^f_{1111} + 10H^f_{1122} + 16H^f_{1133} - 8H^f_{1313} + 2H^f_{3333}\right)$$

$$\tilde{H}^f_{1111} = \frac{1}{30}\left(16H^f_{1111} + 8H^f_{1133} + 16H^f_{1313} + 6H^f_{3333}\right) \tag{5.6}$$

So that effective elastic compliances can be calculated as

$$S^{eff}_{ijkl} = S^0_{ijkl} + \phi_{pores}H^p_{ijkl} + \phi_{fibers}\tilde{H}^f_{ijkl}, \tag{5.7}$$

Where ϕ_{pores} and ϕ_{fibers} are the volume fractions of pores and fibers. Results of the analytical calculation of the effective elastic compliances of FRC are presented in Table 3.

7. Concluding remarks

Analytical approach is based on the property contribution tensor formalism and utilizes Non-Interaction approximation to find overall properties of the structure. Comparison of the effective properties obtained experimentally, analytically and numerically showed an absolute error of ~2.5% for E_3, where lower script "3" specify direction corresponding to the main longitudinal axis. Results of micromechanical calculations and numerical modeling was compared and the discrepancy less than 1 % was identified. The agreement between experiments and simulations is therefore excellent.

Table 3. Effective elastic properties of concrete reinforced with polypropylene fibers obtained using FEM

	FEM	Analytical	Experimental
E_1 ,GPa	1.8766	1.8653	1.9235
E_2 ,GPa	1.8791	1.8653	1.9235
E_3 ,GPa	1.8728	1.8653	1.9235
ν_{12}	0.1029	0.1067	-
ν_{23}	0.1028	0.1067	-
ν_{13}	0.1035	0.1067	-
G_{12} ,GPa	0.8861	0.8427	-
G_{23} ,GPa	0.8878	0.8427	-
G_{23} ,GPa	0.8850	0.8427	-

We conclude that plugging a realistic microstructure description (fiber size, and orientation distributions, pore size distribution) into a customized finite element model produces extremely reliable predictions of the elastic properties of composite materials. Even more, realistic fiber orientation distributions and aspect ratios allow analytical (micromechanical) models to correctly predict such elastic properties. These models represent therefore a valuable tool for the engineer to tailor the concrete properties by knowing its microstructure in some detail. We also show that a detailed knowledge of the microstructure is a competitive quantitative advantage, when tailoring the mechanical properties of composite materials.

Indeed, we predict the above procedure to be in future applicable to other inhomogeneous materials such as ceramic or metal matrix composites.

Acknowledgment

AT acknowledges financial support from RFBR according to the research project № 18-33-00688. IS, GB, and TM acknowledge financial support acknowledge financial support from DFG project BR 5199/3-1.

REFERENCES

[1] V.C. Li, From micromechanics to structural engineering - the design of cementitious composites for civil engineering applications, Doboku Gakkai Rombun-Hokokushu/Proceedings Japan Soc. Civ. Eng. (1993) 1–24.

[2] M.H. Harajli, M.H.. Rtei, Effect of Confinement Using Fiber-Reinforced Polymer or Fiber-Reinforced Concrete on Seismic Performance of Gravity Load-Designed Columns, Struct. J. 101 (2004) 47–56.

[3] L. Yan, C.. Jenkins, R.. Pendleton, Polyolefin fiber-reinforced concrete composites, Cem. Concr. Res. 30 (2000) 391–401. doi:10.1016/S0008-8846(99)00267-7.

[4] L. Lanzoni, A. Nobili, A.M. Tarantino, Performance evaluation of a polypropylene-based draw-wired fibre for concrete structures, Constr. Build. Mater. 28 (2012) 798–806. doi:10.1016/j.conbuildmat.2011.10.017.

[5] S. Wu, Polymer interface and adhesion, M. Dekker, New York, NY, 1982.

[6] A. Bentur, A. Peled, D. Yankelevsky, ENHANCED BONDING OF LOW MODULUS POLYMER FIBERS-CEMENT MATRIX BY MEANS OF CRIMPED GEOMETRY, Cem. Concr. Res. 27 (1997) 1099–1111. doi:10.1016/S0008-8846(97)00088-4.

[7] J.-P. Won, D.-H. Lim, C.-G. Park, Bond behaviour and flexural performance of structural synthetic fibre-reinforced concrete, Mag. Concr. Res. 58 (2006) 401–410. doi:10.1680/macr.2006.58.6.401.

[8] P. Payrow, M.R. Nokken, D. Banu, D. Feldman, Effect of surface treatment on the post-peak residual strength and toughness of polypropylene/polyethylene-blended fiber-reinforced concrete, J. Compos. Mater. 45 (2011) 2047–2054. doi:10.1177/0021998311399481.

[9] P. Di Maida, E. Radi, C. Sciancalepore, F. Bondioli, Pullout behavior of polypropylene macro-synthetic fibers treated with nano-silica, Constr. Build. Mater. 82 (2015) 39–44. doi:10.1016/j.conbuildmat.2015.02.047.

[10] P. Di Maida, C. Sciancalepore, E. Radi, F. Bondioli, Effects of nano-silica treatment on the flexural post cracking behaviour of polypropylene macro-synthetic fibre reinforced concrete, Mech. Res. Commun. 88 (2018) 12–18. doi:10.1016/j.mechrescom.2018.01.004.

[11] E. Radi, L. Lanzoni, A. Sorzia, Analytical Modelling of the Pullout Behavior of Synthetic Fibres Treated with Nano-silica, Procedia Eng. 109 (2015) 525–532. doi:10.1016/j.proeng.2015.06.260.

[12] A. Noushini, B. Samali, K. Vessalas, Effect of polyvinyl alcohol (PVA) fibre on dynamic and material properties of fibre reinforced concrete, Constr. Build. Mater. 49 (2013) 374–383. doi:10.1016/j.conbuildmat.2013.08.035.

[13] A.C. Bordelon, J.R. Roesler, Spatial distribution of synthetic fibers in concrete with X-ray computed tomography, Cem. Concr. Compos. 53 (2014) 35–43. doi:10.1016/j.cemconcomp.2014.04.007.

[14] T. Mishurova, N. Rachmatulin, P. Fontana, T. Oesch, G. Bruno, E. Radi, I. Sevostianov, Evaluation of the probability density of inhomogeneous fiber orientations by computed tomography and its application to the calculation of the effective properties of a fiber-reinforced composite, Int. J. Eng. Sci. 122 (2018) 14–29. doi:10.1016/j.ijengsci.2017.10.002.

[15] H. Rifai, A. Staude, D. Meinel, B. Illerhaus, G. Bruno, In-situ pore size investigations of loaded porous concrete with non-destructive methods, Cem. Concr. Res. (n.d.).

[16] T.S. Oesch, E.N. Landis, D.A. Kuchma, Conventional Concrete and UHPC Performance–

Damage Relationships Identified Using Computed Tomography, J. Eng. Mech. 142 (2016) 4016101. doi:10.1061/(ASCE)EM.1943-7889.0001168.
[17] T. Ponikiewski, J. Gołaszewski, M. Rudzki, M. Bugdol, Determination of steel fibres distribution in self-compacting concrete beams using X-ray computed tomography, Arch. Civ. Mech. Eng. 15 (2015) 558–568. doi:10.1016/j.acme.2014.08.008.
[18] A. Qsymah, R. Sharma, Z. Yang, L. Margetts, P. Mummery, Micro X-ray computed tomography image-based two-scale homogenisation of ultra high performance fibre reinforced concrete, Constr. Build. Mater. 130 (2017) 230–240. doi:10.1016/j.conbuildmat.2016.09.020.
[19] Z. Yang, W. Ren, R. Sharma, S. McDonald, M. Mostafavi, Y. Vertyagina, T.J. Marrow, In-situ X-ray computed tomography characterisation of 3D fracture evolution and image-based numerical homogenisation of concrete, Cem. Concr. Compos. 75 (2017) 74–83. doi:10.1016/j.cemconcomp.2016.10.001.
[20] A. Trofimov, S. Abaimov, I. Akhatov, I. Sevostianov, Effect of elastic contrast on the contribution of helical fibers into overall stiffness of a composites, Int. J. Eng. Sci. 120 (2017). doi:10.1016/j.ijengsci.2017.06.014.
[21] A. Trofimov, I. Sevostianov, The effect of waviness of a helical inhomogeneity on its stiffness- and conductivity contribution tensors, Int. J. Eng. Sci. 116 (2017). doi:10.1016/j.ijengsci.2017.02.008.
[22] B. Drach, I. Tsukrov, A. Trofimov, Comparison of full field and single pore approaches to homogenization of linearly elastic materials with pores of regular and irregular shapes, Int. J. Solids Struct. 96 (2016) 48–63. doi:10.1016/j.ijsolstr.2016.06.023.
[23] A. Trofimov, B. Drach, I. Sevostianov, Effective elastic properties of composites with particles of polyhedral shapes, Int. J. Solids Struct. 120 (2017) 157–170. doi:10.1016/j.ijsolstr.2017.04.037.
[24] A. Trofimov, S. Abaimov, I. Akhatov, I. Sevostianov, On the bounds of applicability of two-step homogenization technique for porous materials, Int. J. Eng. Sci. 123 (2018). doi:10.1016/j.ijengsci.2017.11.017.
[25] M. Muja, D.G. Lowe, FAST APPROXIMATE NEAREST NEIGHBORS WITH AUTOMATIC ALGORITHM CONFIGURATION, in: Proc. Fourth Int. Conf. Comput. Vis. Theory Appl., SciTePress - Science and and Technology Publications, 2009: pp. 331–340. doi:10.5220/0001787803310340.
[26] J.W. Perram, M. Wertheim, Statistical mechanics of hard ellipsoids. I. Overlap algorithm and the contact function, J. Comput. Phys. 58 (1985) 409–416. doi:10.1016/0021-9991(85)90171-8.
[27] H. Horii, S. Nemat-Nasser, Overall moduli of solids with microcracks: Load-induced anisotropy, J. Mech. Phys. Solids. 31 (1983) 155–171. doi:10.1016/0022-5096(83)90048-0.
[28] I.K.M. Sevostianov, Compliance tensors of ellipsoidal inclusions, (1999) L3–L7.
[29] I. Sevostianov, M. Kachanov, On elastic compliances of irregularly shaped cracks, Int. J. Fract. 114 (2002) 245–257. doi:10.1023/A:1015534127172.
[30] M. Kachanov, I. Sevostianov, Micromechanics of Materials, with Applications, 2018. doi:10.1007/978-3-319-76204-3.
[31] I. Sevostianov, F.J. Sabina, Cross-property connections for fiber reinforced piezoelectric materials with anisotropic constituents, Int. J. Eng. Sci. 45 (2007) 719–735. doi:10.1016/j.ijengsci.2007.04.017.